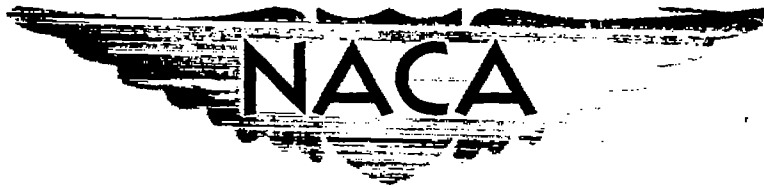


RESTRICTED

RM No. A8H30

NACA RM No. A8H30



RESEARCH MEMORANDUM

WIND-TUNNEL INVESTIGATION OF HORIZONTAL TAILS.

III - UNSWEPT AND 35° SWEPT-BACK

PLAN FORMS OF ASPECT RATIO 6

By Jules B. Dods, Jr.

Ames Aeronautical Laboratory
Moffett Field, Calif.

CLASSIFIED DOCUMENT

This document contains classified information affecting the National Defense of the United States within the meaning of the Espionage Act, USC 5012 and 5013. Its transmission or the revelation of its contents in any manner to an unauthorized person is prohibited by law. Information so classified may be imparted only to persons in the military and naval services of the United States, appropriate civilian officers and employees of the Federal Government who have a legitimate interest therein, and to United States citizens of known loyalty and discretion who of necessity must be informed thereof.

**NATIONAL ADVISORY COMMITTEE
FOR AERONAUTICS**

WASHINGTON
December 17, 1948

RESTRICTED



NATIONAL ADVISORY COMMITTEE FOR AERONAUTICS

RESEARCH MEMORANDUM

WIND-TUNNEL INVESTIGATION OF HORIZONTAL TAILS.

III - UNSWEPT AND 35° SWEEP-BACK PLAN FORMS OF

ASPECT RATIO 6

By Jules B. Dods, Jr.

SUMMARY

The results of a wind-tunnel investigation of the low-speed aerodynamic characteristics of two semispan horizontal tails having unswept and 35° swept-back plan forms are presented. Each model had an aspect ratio of 6, taper ratio of 0.5, and the NACA 64A010 section. The data presented supplement previously reported results of tests of models having the same sections, taper ratio, and sweepback, but with aspect ratios of 3 and 4.5.

Test results are presented for the models with and without standard roughness on their leading edges and with sealed and unsealed radius-nose elevators.

The major effects of sweepback, as measured in the low-speed tests of the two models having an aspect ratio of 6, were to reduce the rate of change of hinge-moment coefficient with angle of attack and with elevator deflection, and to reduce the elevator effectiveness. Roughness increased the maximum lift coefficient of the unswept tail, but practically no effect was noted for the swept-back tail. Removal of the elevator nose seal resulted only in small changes to the lift and hinge-moment parameters.

INTRODUCTION

A systematic investigation of the control-surface characteristics, particularly the hinge-moment parameters, of horizontal-tail surfaces has been undertaken by the NACA to provide experimental results for a comparison with those parameters computed by lifting-surface theory. The investigation was to include a study of the effects

██████████

of sweepback on the horizontal-tail lift and hinge-moment parameters by a comparison of the results of tests of models differing mainly in the angle of sweepback, with the same area, aspect ratio, taper ratio, and section.

In references 1 and 2 the experimental results are presented from wind-tunnel tests of models of aspect ratio 3 and 4.5 without sweep and swept back 35° . The present report extends the experimental data to include an aspect ratio of 6. A comparison of the experimental and theoretical lift and hinge-moment parameters for the models of references 1 and 2 has been presented in reference 3.

COEFFICIENTS AND SYMBOLS

The coefficients and symbols used throughout this report are defined as follows:

Coefficients

C_{he}	elevator hinge-moment coefficient (See appendix.)
C_L	lift coefficient (L/qS)
C_m	pitching-moment coefficient ($M/qS\bar{c}$)
$\frac{\Delta p}{q}$	pressure coefficient across elevator nose seal (pressure below seal minus pressure above seal divided by the dynamic pressure)

Symbols

A	aspect ratio ($2b^2/S$)
b	span of the semispan model measured perpendicular to the plane of symmetry, feet
b_e'	span of the elevator of the semispan model measured along the hinge line, feet
c	chord of the semispan model measured parallel to the plane of symmetry, feet
\bar{c}	mean aerodynamic chord $\left(\frac{\int_0^b c^2 db}{\int_0^b c db} \right)$

c_e	chord of the elevator aft of the hinge line, measured perpendicular to the hinge line, feet
\bar{c}_e	root-mean-square elevator chord aft of the hinge line measured parallel to the plane of symmetry, feet
\bar{c}_e'	root-mean-square elevator chord aft of the hinge line measured perpendicular to the hinge line, feet
H	moment about hinge line, foot-pounds
L	lift, pounds
M	pitching moment about a lateral axis through the 0.25 \bar{c} point, foot-pounds
M_A	first moment of the elevator area aft of the hinge line about the hinge line, feet cubed
q	free-stream dynamic pressure ($\frac{1}{2}\rho V^2$), pounds per square foot
R	Reynolds number ($\rho V \bar{c} / \mu$)
S	area of semispan horizontal tail, square feet
S_e	area of semispan elevator aft of hinge line, square feet
V	velocity of air, feet per second
α	corrected angle of attack, degrees
δ_e	elevator deflection (positive when trailing edge of elevator is down), measured in a plane normal to the hinge line, degrees
μ	absolute viscosity, slugs per foot-second
ρ	density of air, slugs per cubic foot

Parameters

$$\alpha_{\delta_e} = - \frac{C_{L\delta_e}}{C_{L\alpha}} \quad \text{elevator-effectiveness parameter}$$

$$C_{h\alpha} = \left(\frac{\partial C_{h_e}}{\partial \alpha} \right)_{\delta_e = 0} \quad (\text{measured through } \alpha = 0)$$

$$C_{n\delta_e} = \left(\frac{\partial C_{n_e}}{\partial \delta_e} \right)_{\alpha = 0} \quad (\text{measured through } \delta_e = 0)$$

$$C_{l\alpha} = \left(\frac{\partial C_l}{\partial \alpha} \right)_{\delta_e = 0} \quad (\text{measured through } \alpha = 0)$$

$$C_{l\delta_e} = \left(\frac{\partial C_l}{\partial \delta_e} \right)_{\alpha = 0} \quad (\text{measured through } \delta_e = 0)$$

MODELS

The semispan, or reflection-plane, models tested in this investigation had an aspect ratio of 6 and a taper ratio (ratio of tip chord to root chord) of 0.5. The 0.25-chord line was swept back 5.7° for the "unswept" model and 35° for the swept-back model, as shown in figure 1.

The NACA 64A010 airfoil section was perpendicular to the 0.70-chord line (elevator hinge line) for the unswept model and perpendicular to the 0.25-chord line for the swept-back model. The airfoil section was the same as for the models of references 1 and 2. (The slight discrepancies between the model coordinates and the true 64A010 coordinates (table I) are not considered important.)

Both models were equipped with sealed radius-nose elevators. For the unswept model the elevator chord aft of the hinge line was 0.30 of the chord perpendicular to the 0.70-chord line. The elevator chord of the swept-back model was 0.30 of the chord perpendicular to the 0.25-chord line. Because the elevator-chord ratios were held constant in the manner explained previously, the ratios of elevator area to total-surface area were different — 0.300 for the unswept model and 0.278 for the swept-back model.

The gaps between the elevators and the shrouds and the gaps between the elevator noses and the balance plates (seal gap) are shown in figure 1. The elevator nose gaps were sealed spanwise from the root to the tip. Pressure orifices were located in the balance chambers enclosed by the shrouds both above and below the seal at four spanwise stations. The ends of the balance chamber were sealed at the root and at the hinge brackets. The elevator hinge brackets on both models were located immediately below the tunnel floor, and at 82-percent span. An additional bracket was placed at 38-percent span of the swept-back model. The balance-chamber pressure orifices at 91-percent span were, therefore, outboard of the hinge brackets.

The tip shapes were formed by rotating the tip airfoil section parallel to the undisturbed air stream about a line inboard of the tip, a distance equal to the maximum tip ordinate.

Photographs showing the models mounted in the wind tunnel are presented in figures 2 and 3.

TESTS

The models were mounted on a turntable flush with the floor of one of the Ames 7- by 10-foot wind tunnels. (See figs. 2 and 3.) The tests were conducted with a dynamic pressure of 75.5 pounds per square foot, corresponding to a Reynolds number of 3.0×10^6 . The models were tested in the smooth condition with the elevator sealed, unless otherwise specified. For those tests with leading-edge roughness, standard roughness was applied as defined in reference 4.

Model lift and pitching moment were measured by means of the wind-tunnel balance system. The elevator hinge moment was measured by means of a resistance-type torsional strain gage. Pressures above and below the elevator nose seal in the balance chamber were measured by the use of a manometer connected to the orifices in the balance chamber.

CORRECTIONS

All coefficients and the angle of attack have been corrected for the effects of the tunnel walls. The method for computing the corrections was similar to that of reference 5. The corrections listed below were added to the data for both the unswept and the swept-back models:

$$\Delta\alpha_1 = 0.994 C_{L_u}$$

$$\Delta\alpha_2 = 0.0933 C_{L_u} (\delta_e = 0)$$

$$\Delta C_m = 0.00274 C_{L_u}$$

$$\Delta C_{h_e} = 0.00358 C_{L_u}$$

$$C_L = 0.993 C_{L_u}$$

where

- $\Delta\alpha_1$ jet-boundary correction to angle of attack
- $\Delta\alpha_2$ streamline-curvature correction to angle of attack
- ΔC_m correction to pitching-moment coefficient
- ΔC_{h_e} correction to hinge-moment coefficient
- C_{L_u} uncorrected lift coefficient

RESULTS AND DISCUSSION

The results of tests of the unswept model are presented in figures 4 to 8, and those for the swept-back model are presented in figures 9 to 13. The variations of lift, hinge-moment, and pitching-moment coefficients with angle of attack for various elevator deflections are given in figures 4 and 9. Hinge-moment coefficients are also shown as a function of elevator deflection for various angles of attack in figures 5 and 10. The variation of the pressure coefficient across the elevator nose seal with angle of attack is presented in figures 6 and 11. The effects of standard roughness and removal of the elevator nose seal on the lift and hinge-moment coefficients are shown in figures 7 and 8 for the unswept model and in figures 12 and 13 for the swept-back model.

Effectiveness and Hinge-Moment Parameters

The lift effectiveness and the hinge-moment parameters are listed in table II for the two models. As shown by this table, C_{h_α} changed from -0.0030 for the unswept model to -0.0028 for the swept-back model; the change in $C_{h_{\delta_e}}$ was from -0.0104 to -0.0072, and the elevator-effectiveness parameter α_{δ_e} was changed from -0.68 to -0.52. The value of $C_{L_{\delta_e}}$ was reduced from 0.050 to 0.034, and C_{L_α} was reduced from 0.074 to 0.065. Although the major part of the change in the parameters can be attributed to sweepback, the possibility of effects due to the difference between the ratio of elevator area to total-surface area for the unswept and the swept-back models should be noted.

Static Longitudinal Stability

The variation of pitching-moment coefficient with angle of attack indicates a stabilizing effect of sweepback; the aerodynamic center was shifted aft about 2 percent of the mean aerodynamic chord. The unswept model was statically unstable near zero lift coefficient [$(dC_m/d\alpha)_{\delta_e=0} = 0.0016$], while the swept-back model was neutrally stable, as shown in figures 4(c) and 9(c).

The experimental results presented in figures 4(c) and 9(c) also confirm the predictions of reference 6 that at the stall the static longitudinal stability of the unswept model would increase and that the swept-back model would be unstable.

Effect of Standard Roughness

The effects of standard leading-edge roughness (elevator sealed) upon the lift and hinge-moment coefficients are shown in figure 7 for the unswept model and in figure 12 for the swept-back model.

Standard roughness on the unswept model increased the maximum lift coefficient by 0.11 with the elevator undeflected, and by approximately the same amount with the elevator deflected either down 4° or up 15° . These increases were obtained primarily because the stall occurred at a higher angle of attack. The presence of roughness also increased the angle of attack at which the hinge-moment coefficients diverged. The value of $C_{h\alpha}$ of -0.0030 for the unswept model in the smooth condition was changed to -0.0036 by the addition of standard roughness, and $C_{h\delta_e}$ was changed from -0.0104 to -0.0100.

Standard roughness on the swept-back tail had only small effects on the maximum lift coefficient for any elevator deflection. The angle of attack at which the hinge-moment coefficients increased rapidly was extended slightly by roughness. The value of $C_{h\alpha}$ (measured in the linear range) for the swept-back tail in the smooth condition was unchanged by roughness, but $C_{h\delta_e}$ was changed from -0.0072 to -0.0067.

As shown in figure 4(a), a different type of stall was measured for the unswept model at positive and negative angles of attack. A similar result was found for the unswept models of aspect ratios 3 and 4.5. Measurements have shown the model twist under load to

be negligible and the airfoil contours to be satisfactory. Additional tests of the unswept model of aspect ratio 3 (reference 1) at Reynolds numbers from 2.2 to 4.4×10^6 indicated that Reynolds numbers within that range had no effect upon the type of stall, that is, whether the stall was gradual or abrupt. Since the more gradual type of stall was measured at positive angles of attack for the aspect ratio 4.5 and 6 models, and at negative angles of attack for the aspect ratio 3 model, there does not appear to be any excessive asymmetry of the air stream. Thus, the reason for the two types of stall is unexplained.

Effect of Removing Elevator Nose Seal

As shown in table II and in figures 8 and 13, removing the elevator nose seal (models in the smooth condition) produced small changes in the lift and hinge-moment parameters near zero elevator deflection and angle of attack, and somewhat larger changes in the hinge-moment coefficients at the higher elevator deflections and angles of attack.

CONCLUSIONS

The results of tests conducted to evaluate the low-speed aerodynamic characteristics of horizontal tails with an aspect ratio of 6 having unswept and swept-back plan forms indicated that:

1. The value of $C_{h\alpha}$ was changed from -0.0030 for the unswept tail to -0.0028 for the 35° swept-back tail.
2. The value of $C_{h\delta}$ was changed from -0.0104 for the unswept tail to -0.0072 for the 35° swept-back tail.
3. The elevator-effectiveness parameter α_{δ} was changed from -0.68 for the unswept tail to -0.52 for the swept-back tail.
4. Sweepback had a stabilizing effect on the static longitudinal stability. The aerodynamic center was shifted aft about 2 percent of the mean aerodynamic chord.
5. Standard leading-edge roughness increased the maximum lift coefficient of the unswept tail, but practically no effect was noted for the swept-back tail.

6. Removal of the elevator nose seal resulted only in small changes to the lift and hinge-moment parameters.

Ames Aeronautical Laboratory,
National Advisory Committee for Aeronautics,
Moffett Field, Calif.

APPENDIX

Conversion Factors for Hinge-Moment Coefficients

Because several methods are in use for the conversion of hinge moments to nondimensional coefficient form, particularly for swept-back lifting surfaces, factors relating the various methods are presented. To obtain the hinge-moment coefficients for one of the listed methods, multiply the value of the hinge-moment coefficients of this report by the corresponding factor in the following table:

Equations for hinge-moment coefficients	Unswept model		Swept-back model	
	$\frac{H}{qC_{h_e}}$ (ft ³)	Conversion factor	$\frac{H}{qC_{h_e}}$ (ft ³)	Conversion factor
$C_{h_e} = \frac{H}{qS_e\bar{c}_e}$	1.694	1.000	1.455	1.000
$C_{h_e} = \frac{H}{qb\bar{c}_e^2}$	1.725	.982	1.482	.982
$C_{h_e} = \frac{H}{qb_e'(\bar{c}_e')^2}$	1.725	.982	1.271	1.145
$C_{h_e} = \frac{H}{2qM_A}$	1.725	.982	1.271	1.145

REFERENCES

1. Dods, Jules B., Jr.: Wind-Tunnel Investigation of Horizontal Tails. I - Unswept and 35° Swept-Back Plan Forms of Aspect Ratio 3. NACA RM No. A7K24, 1947.
2. Dods, Jules B., Jr.: Wind-Tunnel Investigation of Horizontal Tails. II - Unswept and 35° Swept-Back Plan Forms of Aspect Ratio 4.5. NACA RM No. A8B11, 1948.
3. Jones, Arthur L., and Sluder, Loma: An Application of Falkner's Surface-Loading Method to Predictions of Hinge-Moment Parameters for Swept-Back Wings. NACA TN No. 1506, 1948.
4. Abbott, Ira H., von Doenhoff, Albert E., and Stivers, Louis S., Jr.: Summary of Airfoil Data. NACA Rep. No. 824, 1945.
5. Swanson, Robert S., and Toll, Thomas A.: Jet-Boundary Corrections for Reflection-Plane Models in Rectangular Wind Tunnels. NACA Rep. No. 770, 1943.
6. Shortal, Joseph A., and Maggin, Bernard: Effect of Sweepback and Aspect Ratio on Longitudinal Stability Characteristics of Wings at Low Speeds. NACA TN No. 1093, 1946.

TABLE I.—COORDINATES FOR THE NACA 64A010
AIRFOIL AND THE MODELS TESTED

[All Dimensions in Percent of Wing Chord]

Upper and Lower Surfaces		
Station	NACA 64A010 ordinate	Model ordinate
0	0	0
.50	.804	.819
.75	.969	.987
1.25	1.225	1.247
2.50	1.688	1.696
5.00	2.327	2.333
7.50	2.805	2.780
10.00	3.199	3.202
15.00	3.813	3.816
20.00	4.272	4.280
25.00	4.606	4.610
30.00	4.837	4.842
35.00	4.968	4.950
40.00	4.995	4.975
45.00	4.894	4.889
50.00	4.684	4.672
55.00	4.388	4.373
60.00	4.021	4.011
65.00	3.597	3.594
70.00	3.127	3.131
75.00	2.623	2.637
80.00	2.103	2.120
85.00	1.582	1.595
90.00	1.062	1.071
95.00	.541	.553
100.00	.021	0
L.E. radius 0.687 ^a T.E. radius 0.023 ^a		

^aSame for both the NACA 64A010 section
and the model.



TABLE II.— A SUMMARY OF THE LIFT AND HINGE-MOMENT
PARAMETERS OF THE UNSWEPT AND 35° SWEEP-BACK
MODELS OF ASPECT RATIO 6
[R, 3.0×10^3]

Parameter	Model Condition		
	Model smooth; elevator sealed	Model with standard roughness; elevator sealed	Model smooth; elevator seal removed
Unswept			
$C_{h\alpha}$	-0.0030	-0.0036	-0.0032
$C_{h\delta_e}$	-.0104	-.0100	-.0109
$C_{L\alpha}$.074	.075	.073
$C_{L\delta_e}$.050	.048	.049
α_{δ_e}	-.68	-.64	-.67
Swept back			
$C_{h\alpha}$	-0.0028	-0.0028	-0.0027
$C_{h\delta_e}$	-.0072	-.0067	-.0074
$C_{L\alpha}$.065	.066	.065
$C_{L\delta_e}$.034	.031	.033
α_{δ_e}	-.52	0-.47	-.51



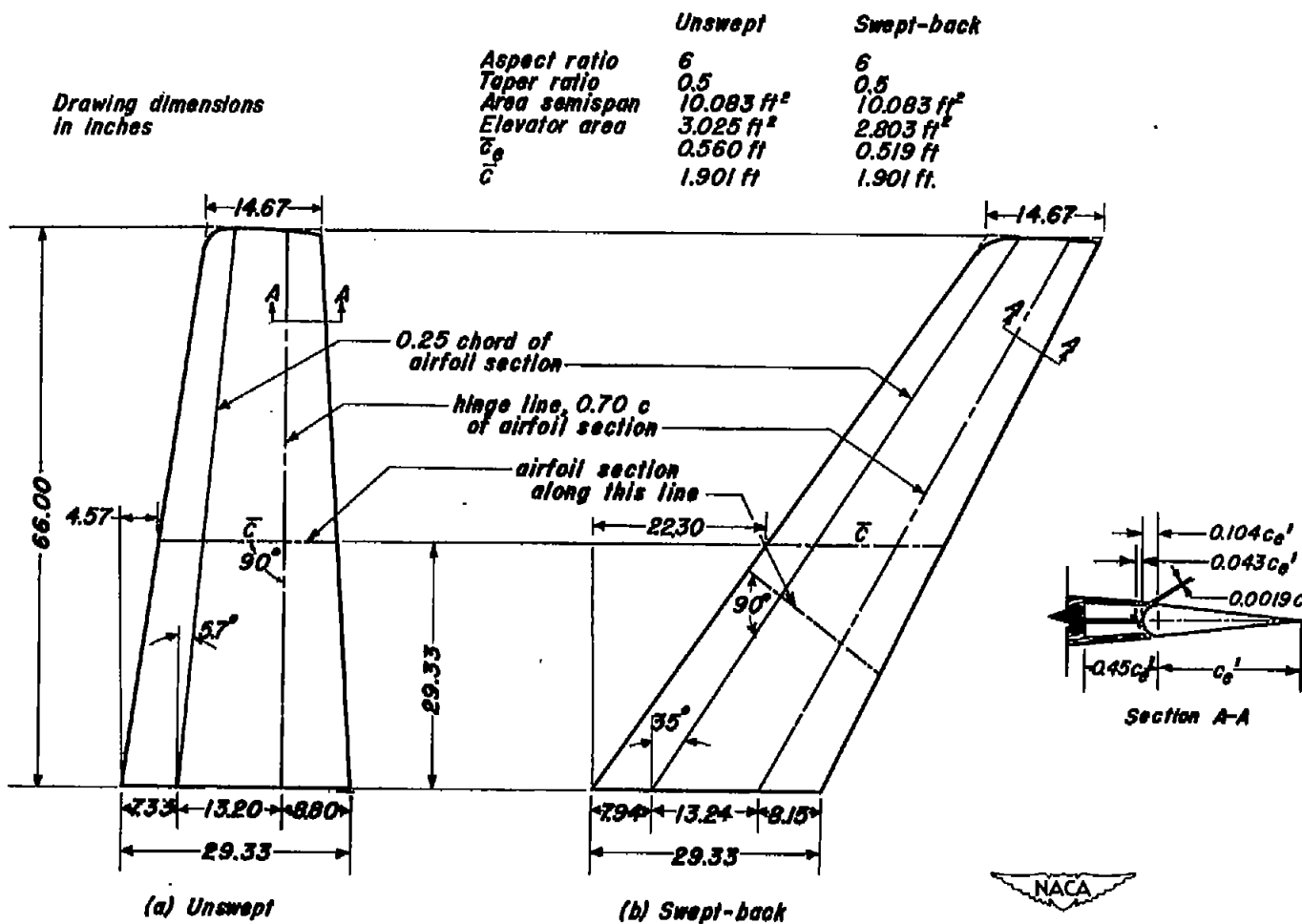


Figure 1.— Plan forms of the horizontal tail models of aspect ratio 6.



(a) Three-quarter front view.



(b) Three-quarter rear view.

Figure 2.— The unswept tail mounted in the 7- by 10-foot wind tunnel.

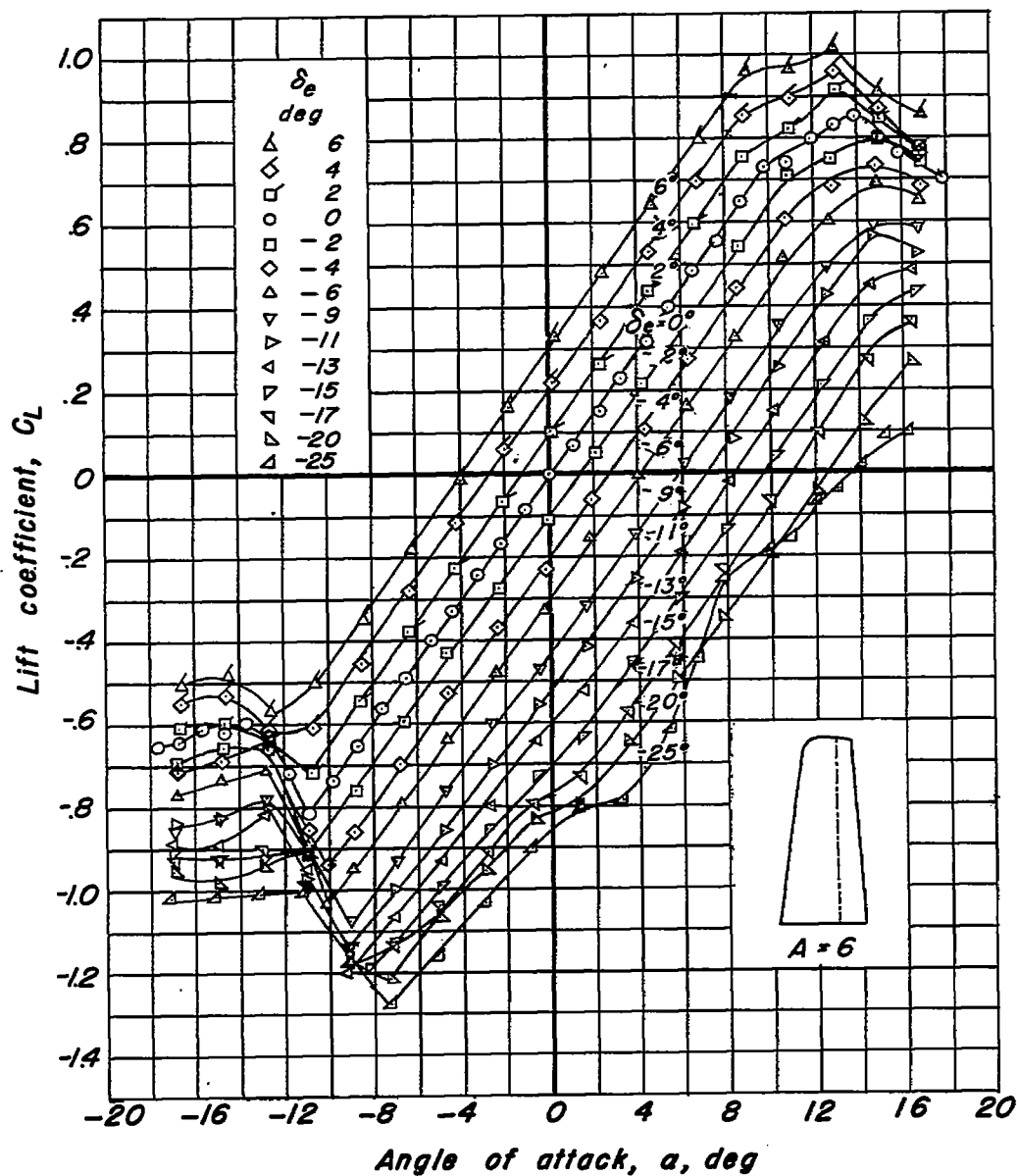


(a) Three-quarter front view.



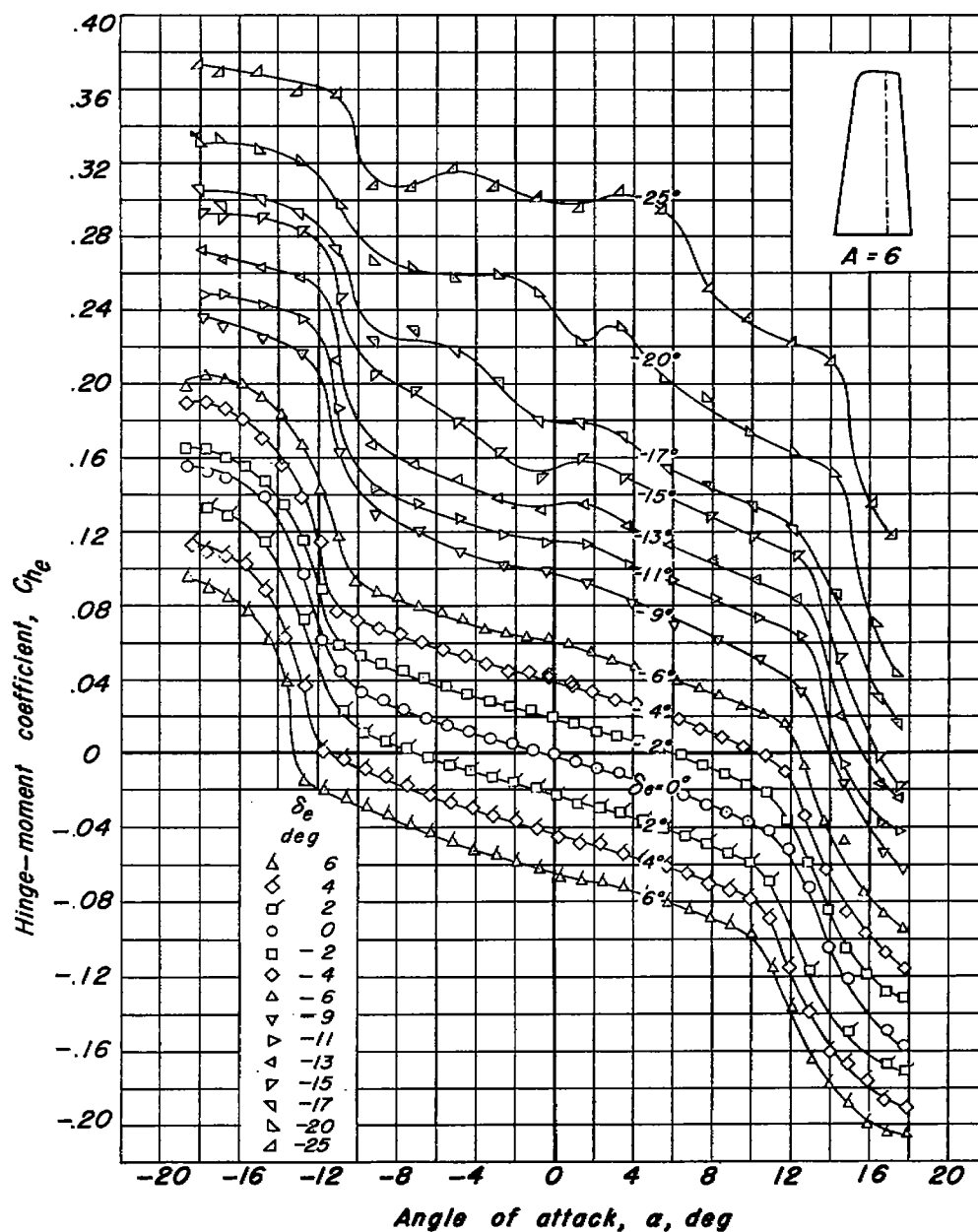
(b) Three-quarter rear view.

Figure 3.— The 35° swept-back tail mounted in the 7- by 10-foot wind tunnel.



(a) Lift coefficient.

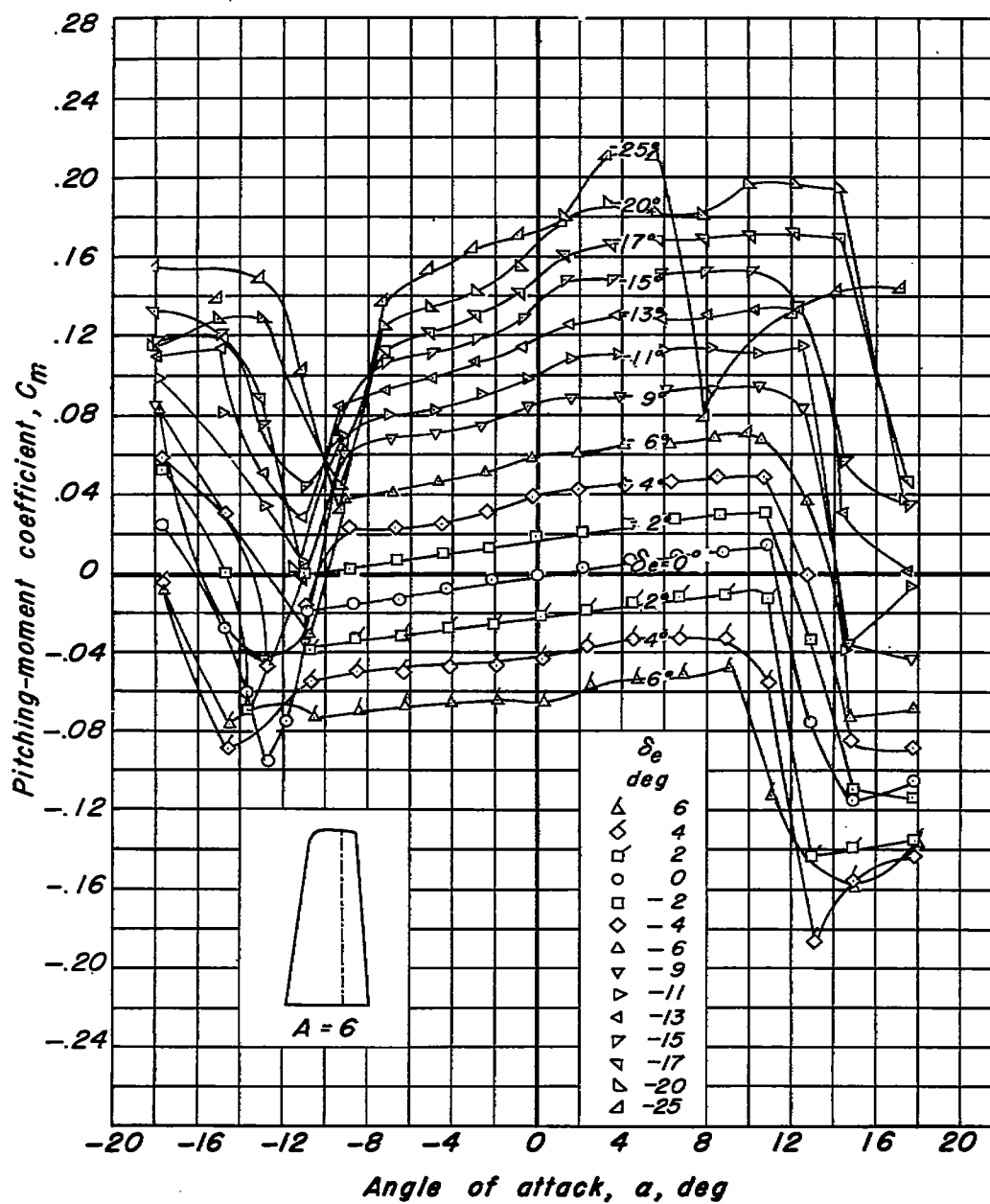
Figure 4.— Lift, hinge-moment, and pitching-moment coefficients of the unswept tail. Aspect ratio, 6; $R, 3.0 \times 10^6$.



(b) Hinge-moment coefficient.

NACA

Figure 4.-Continued.



(c) Pitching-moment coefficient.

Figure 4- Concluded.

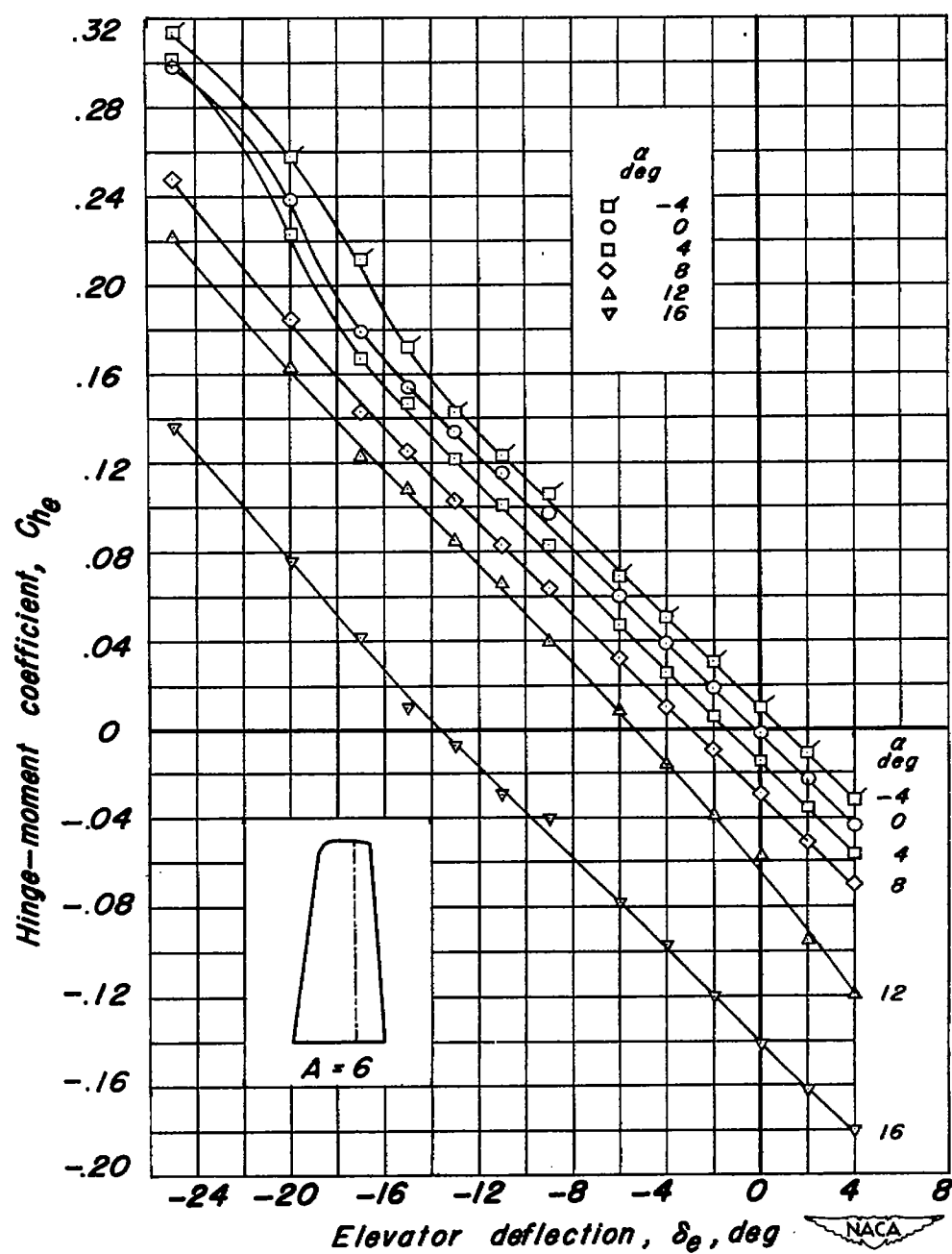
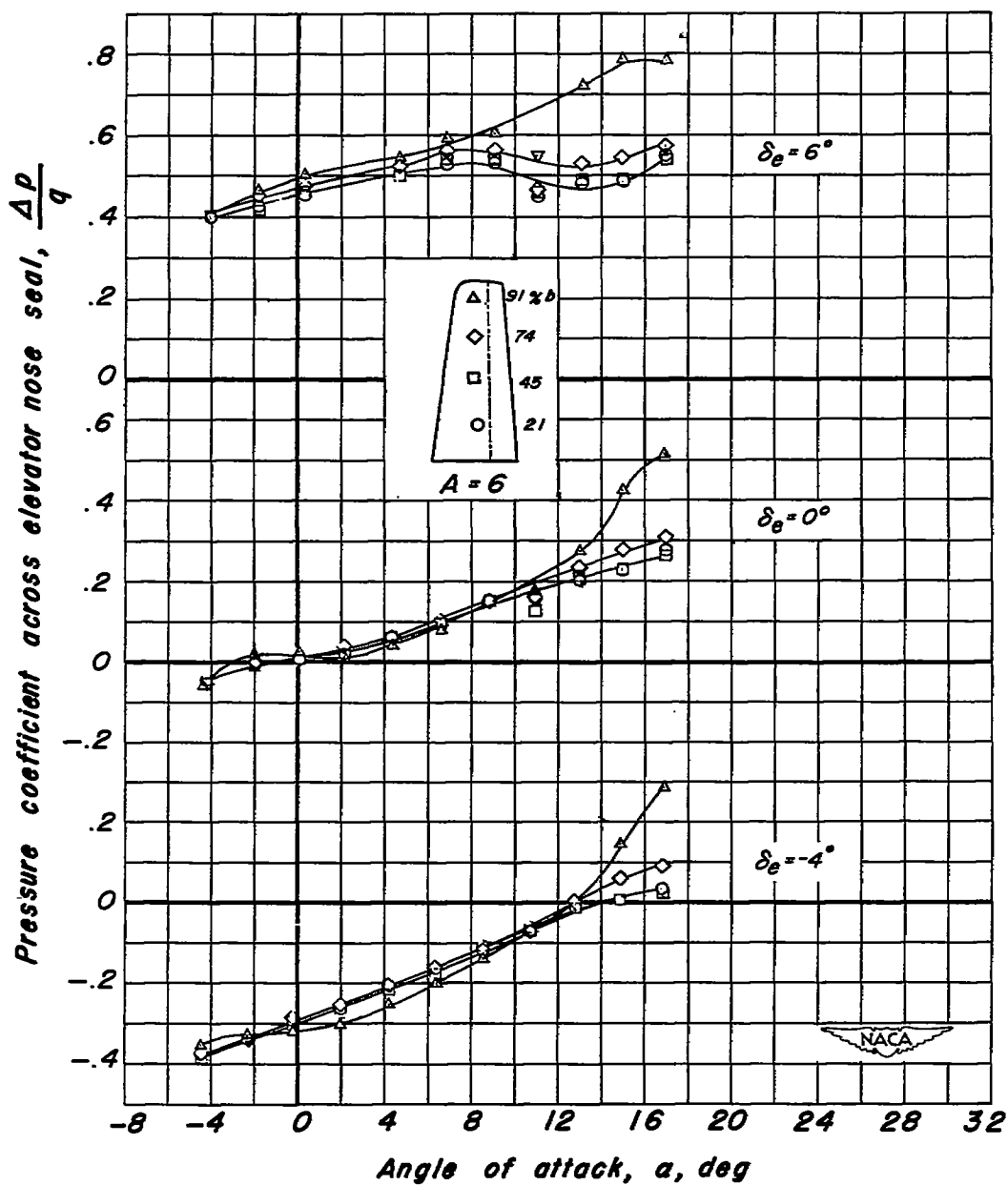
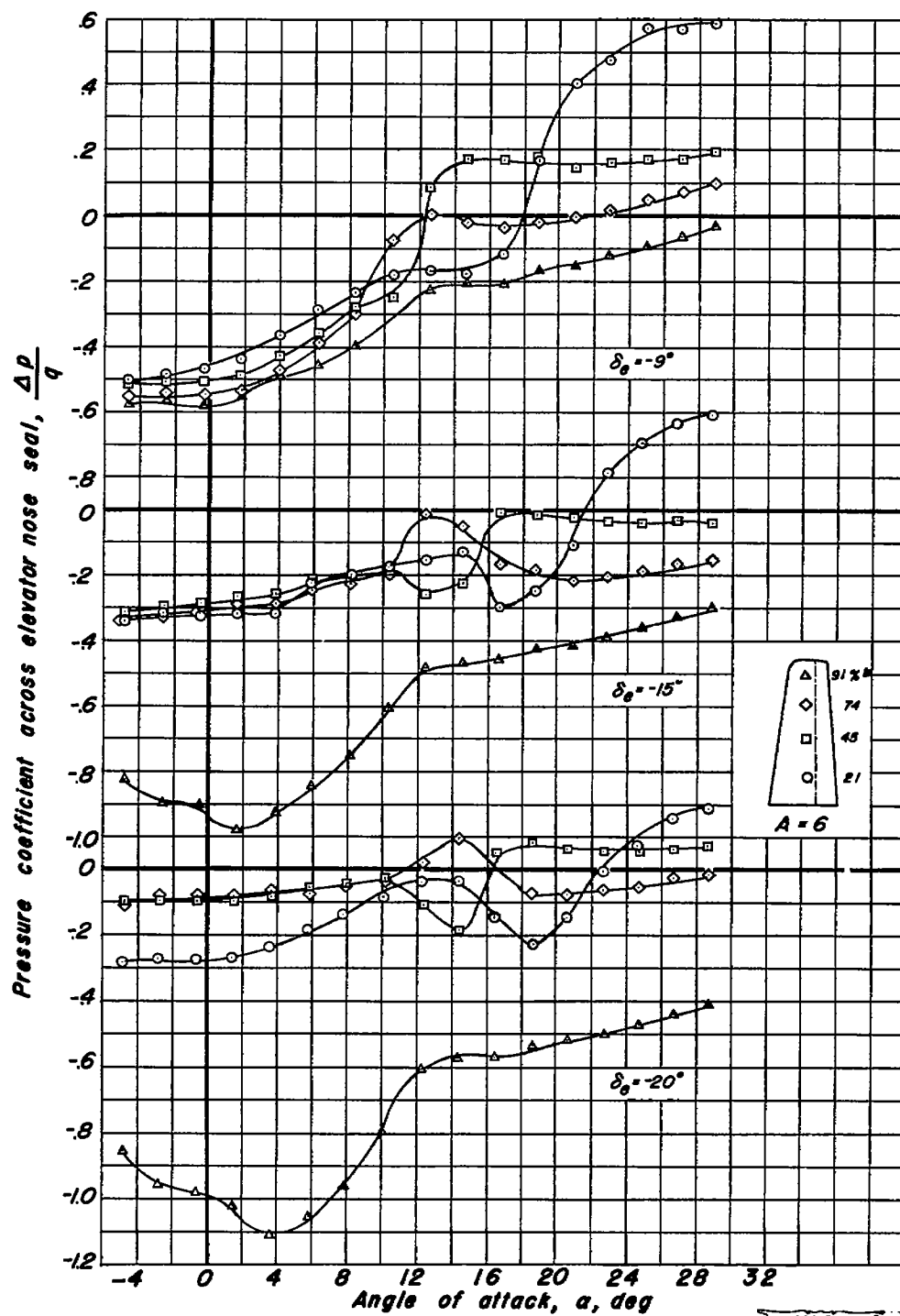


Figure 5.- Variation of hinge-moment coefficient with elevator deflection for various angles of attack of the unswept tail. Aspect ratio, 6; $R, 3.0 \times 10^6$.



(a) $\delta_e = 6^\circ, 0^\circ, -4^\circ$

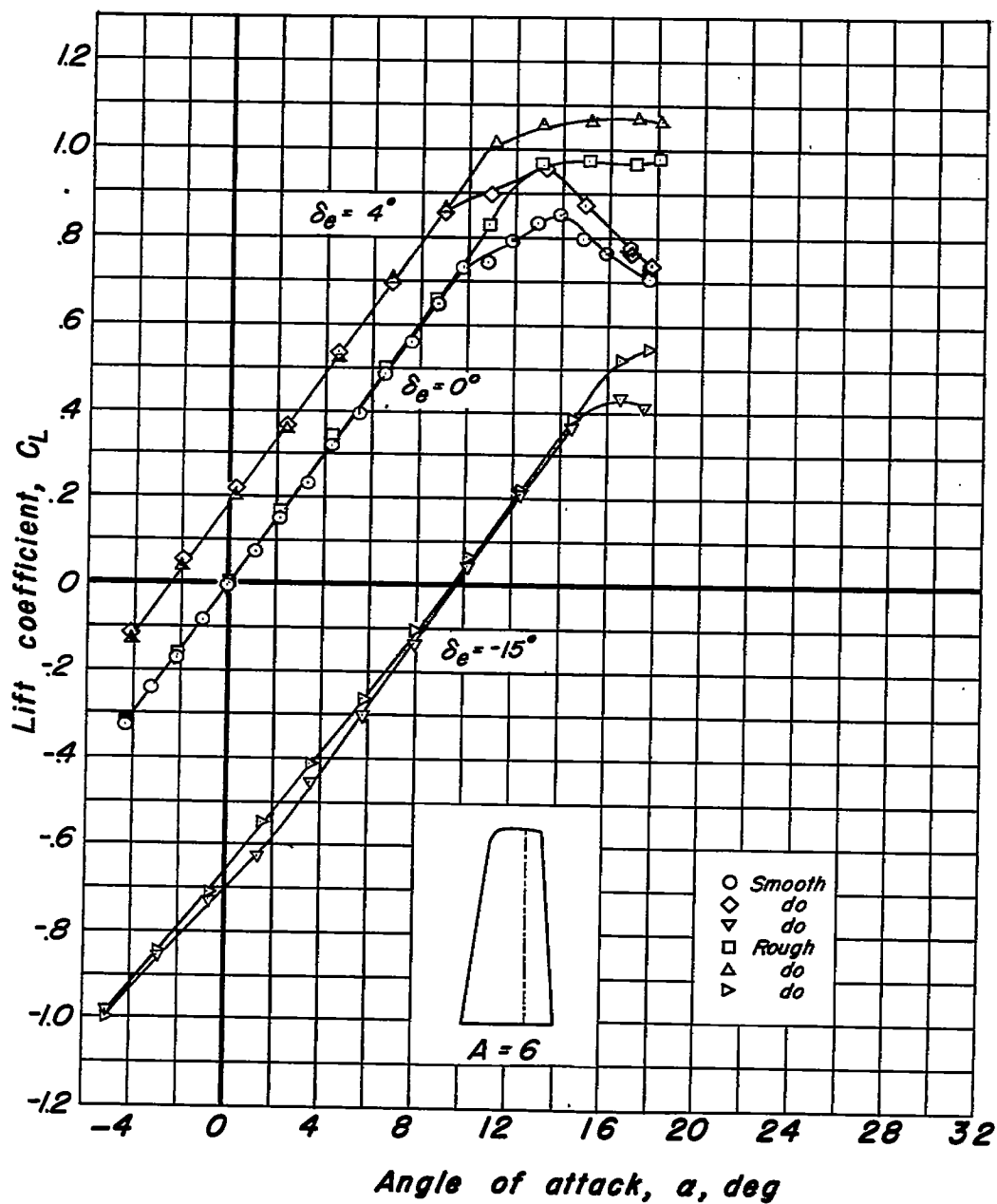
Figure 6.- Variation of pressure coefficient across elevator nose seal with angle of attack of the unswept tail. Aspect ratio, 6; $R, 3.0 \times 10^6$.



(b) $\delta_0 = -9^\circ, -15^\circ, -20^\circ$

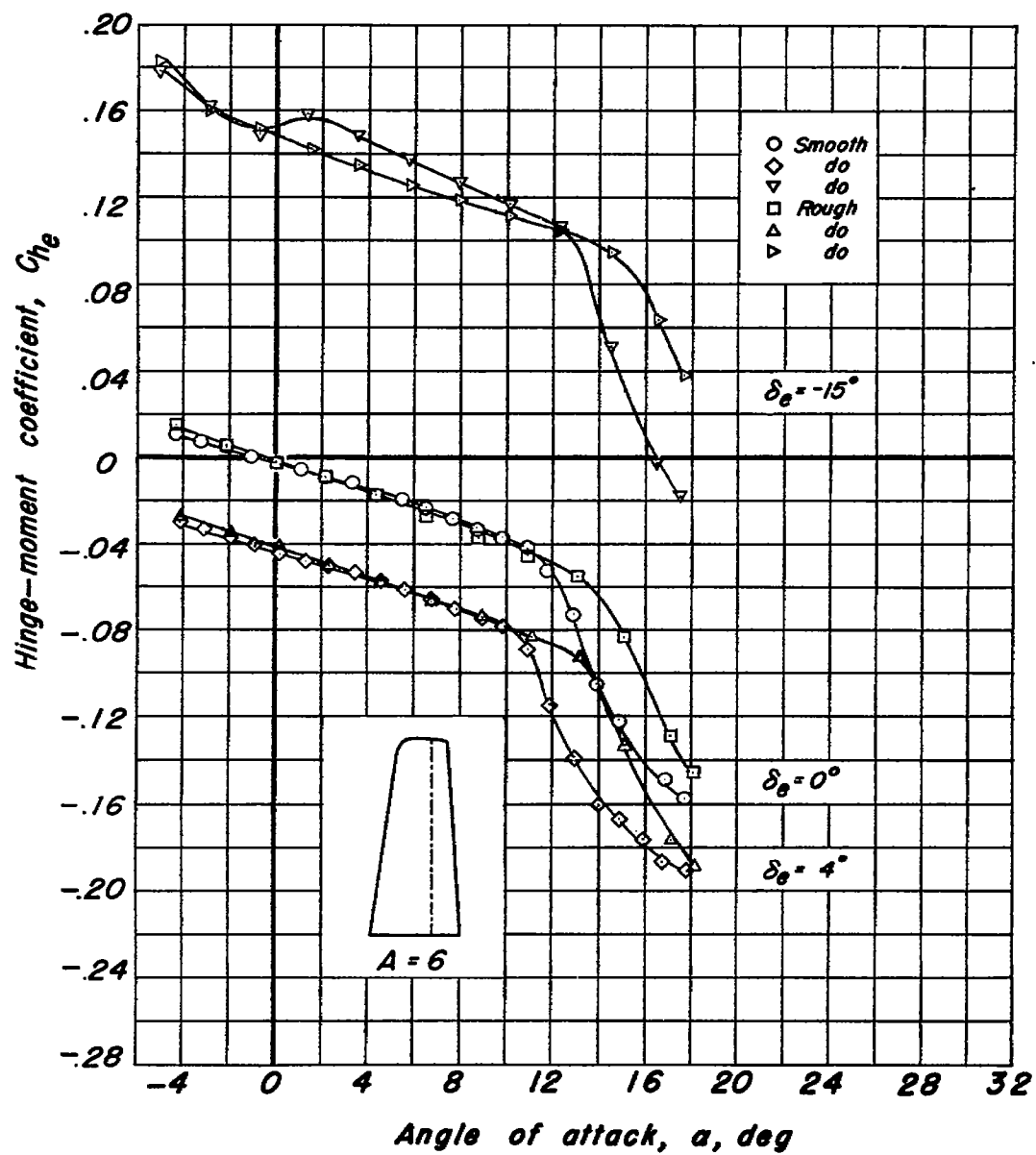
Figure 6-Concluded.





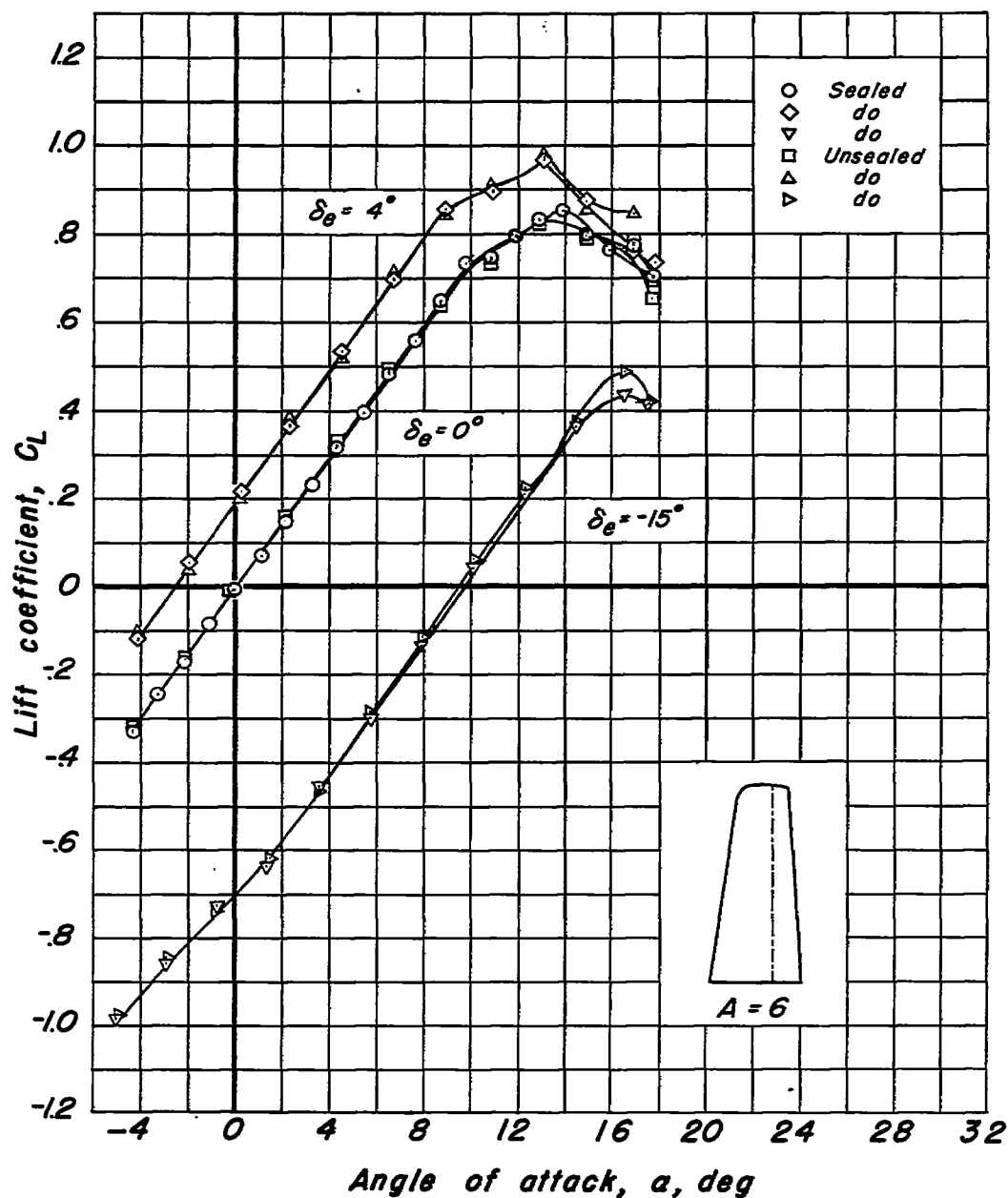
(a) Lift coefficient.

Figure 7.- Comparison of the lift and hinge-moment coefficients with and without leading-edge roughness on the unswept tail. Aspect ratio, 6; R , 3.0×10^6 .



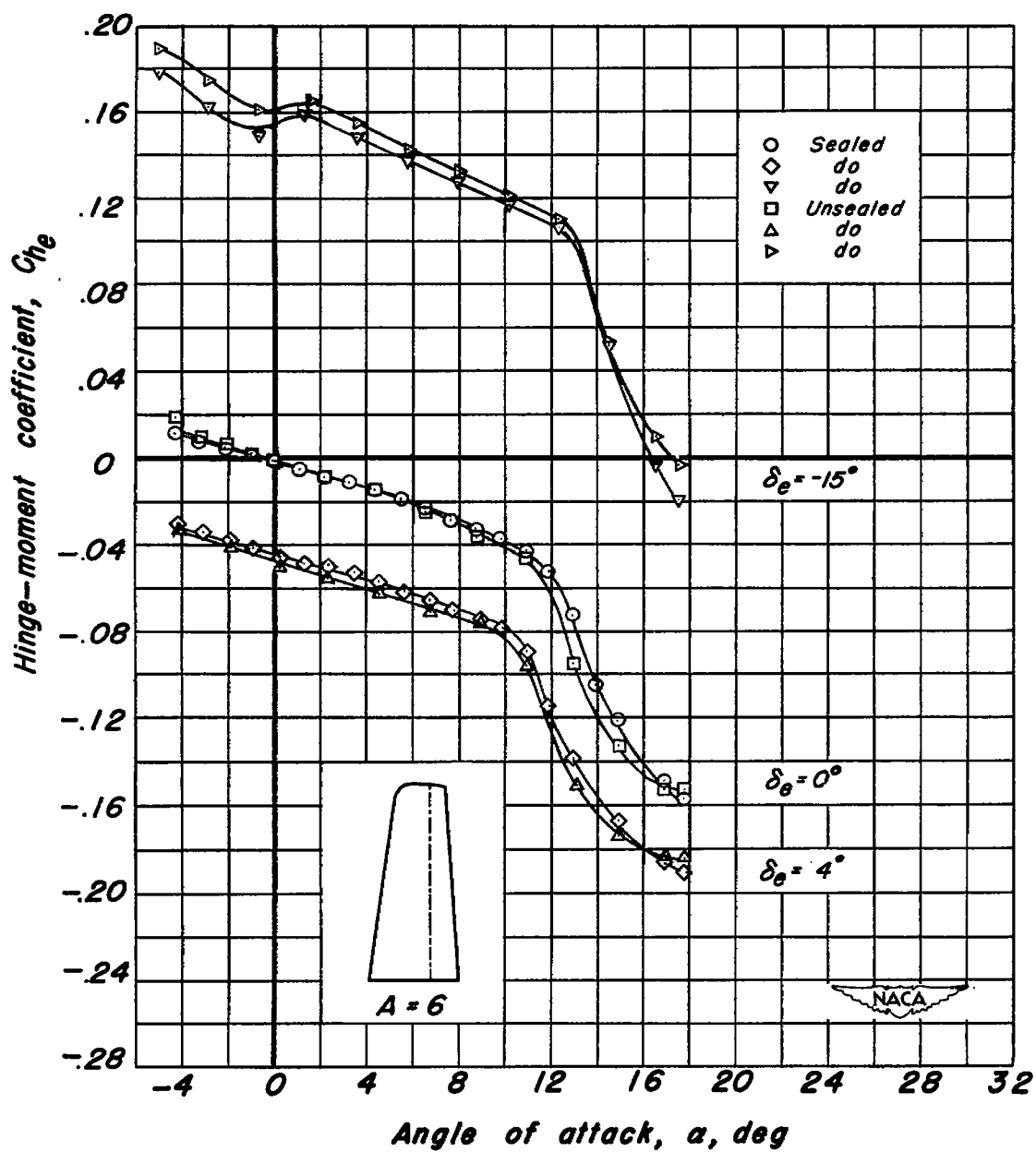
(b) Hinge-moment coefficient.

Figure 7.—Concluded.



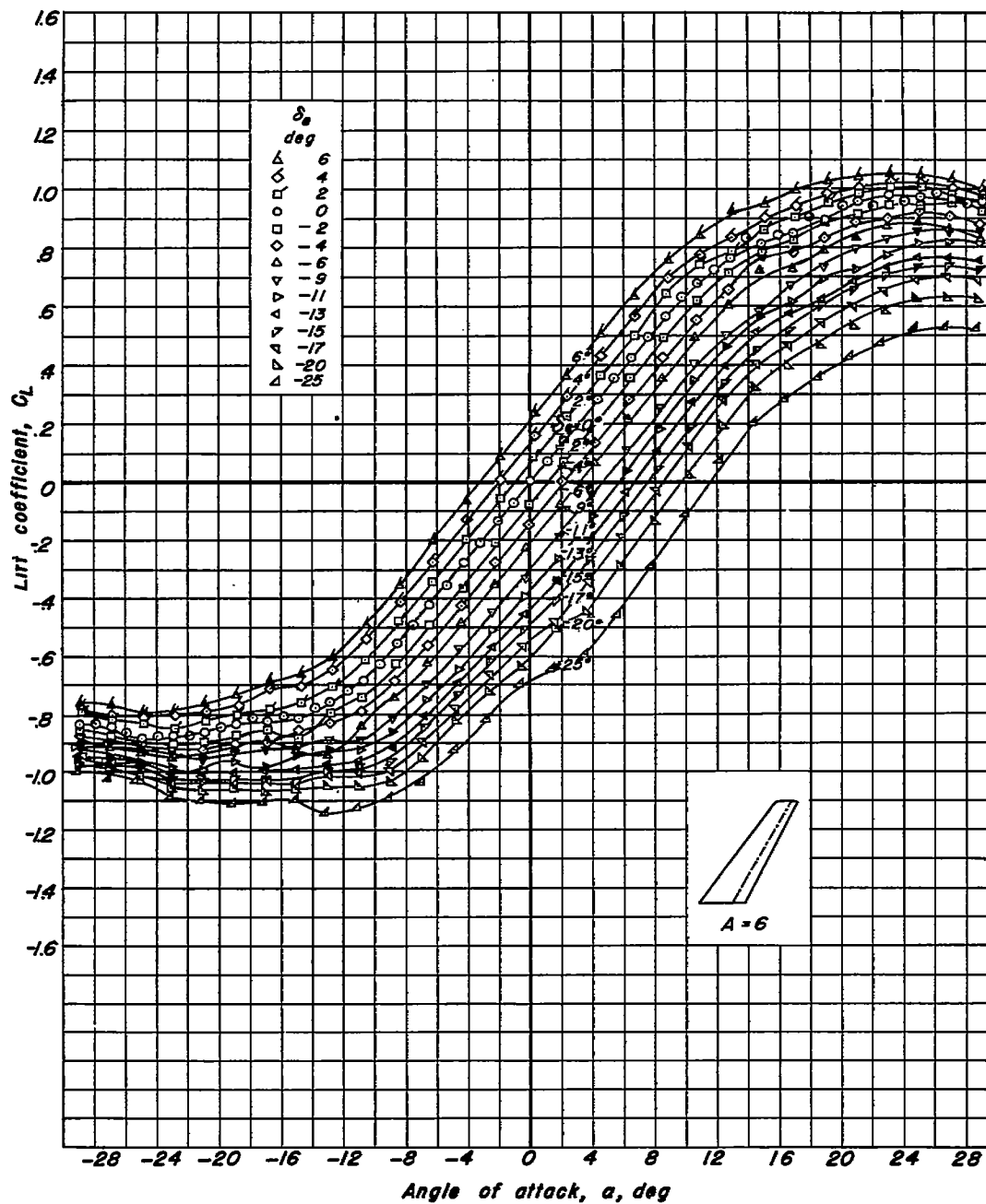
(a) Lift coefficient.

Figure 8:- Comparison of the lift and hinge-moment coefficients with and without elevator seal on the unswept tail. Aspect ratio, 6; $R, 3.0 \times 10^6$.



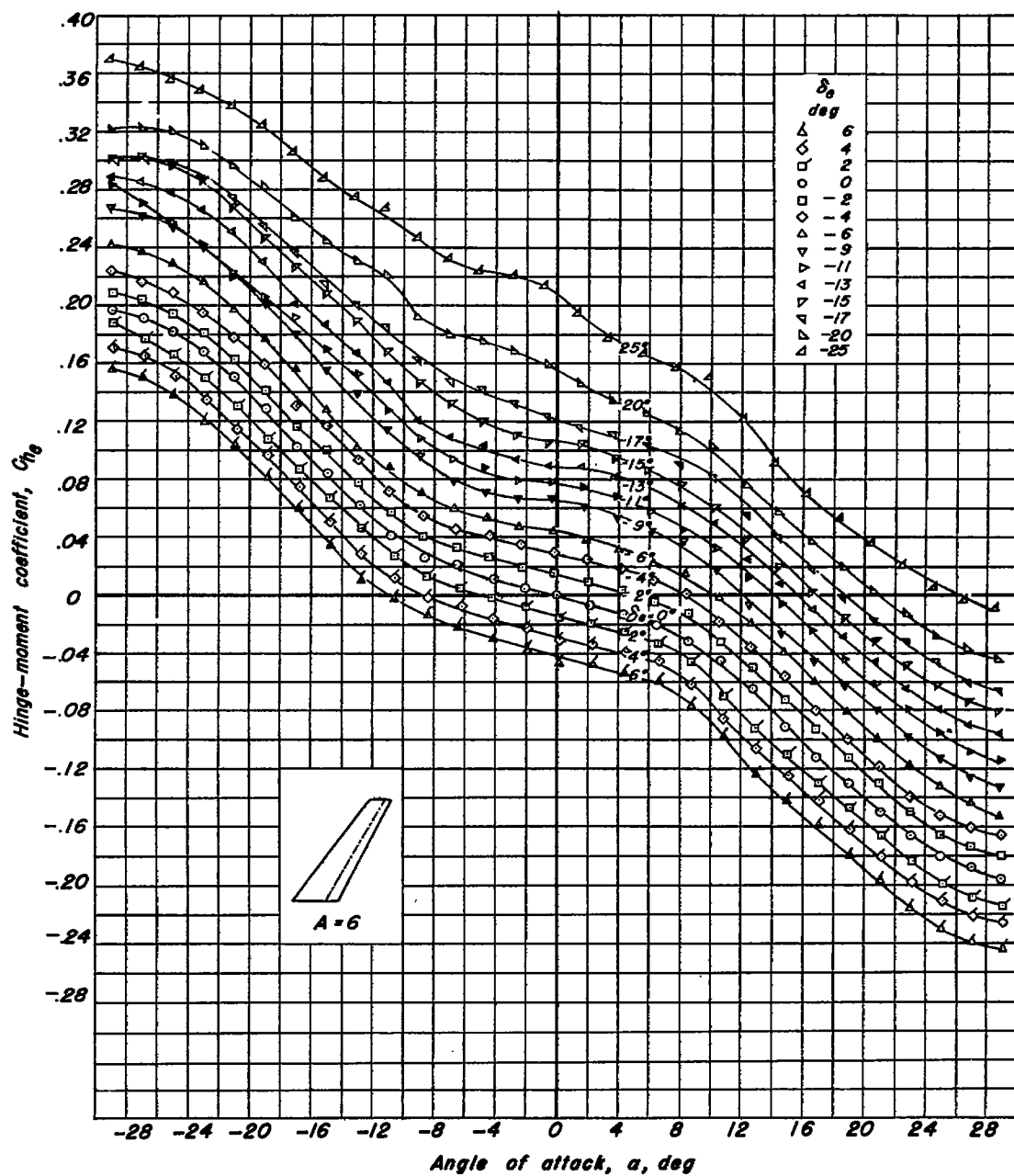
(b) Hinge-moment coefficient.

Figure 8.-Concluded.



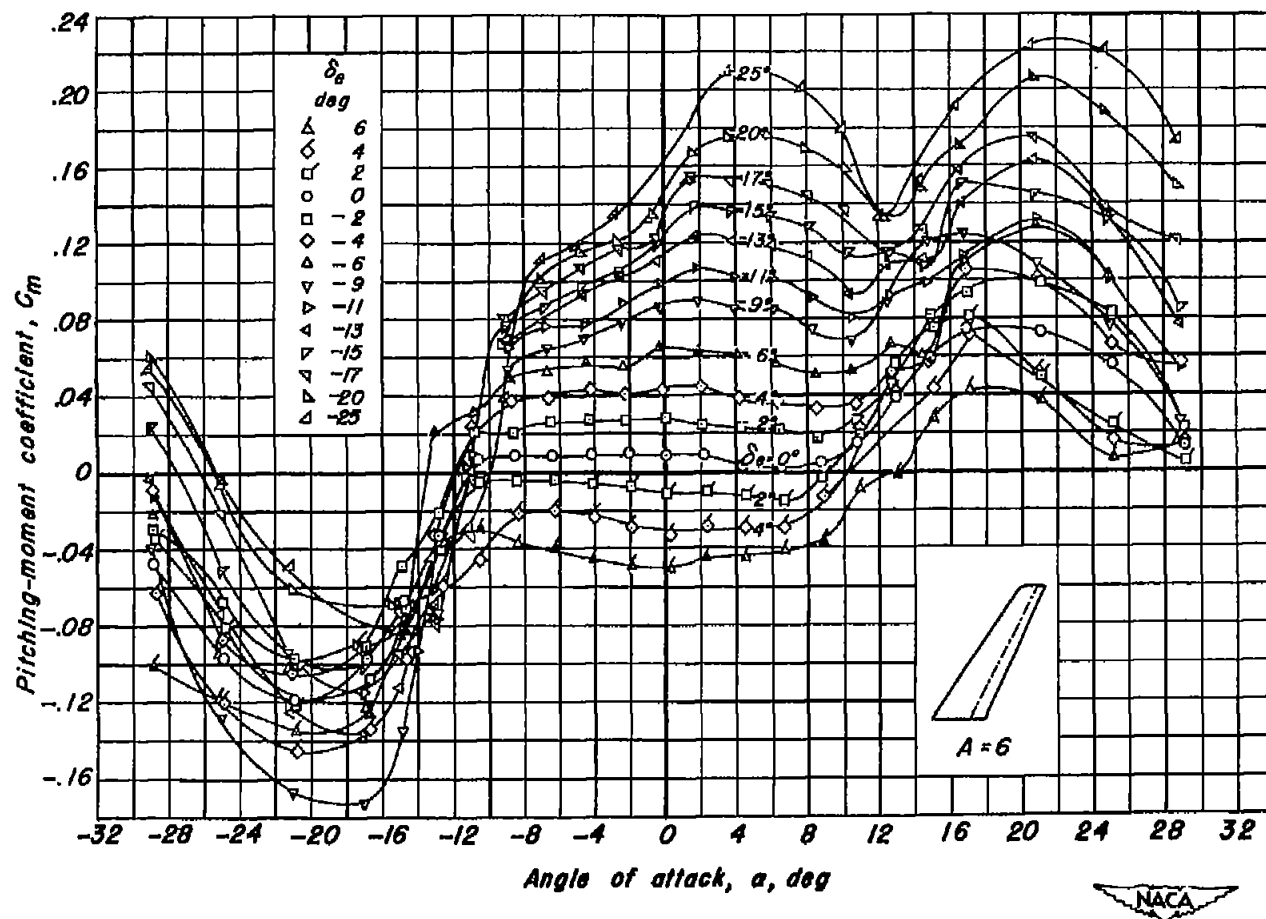
(a) Lift coefficient.

Figure 9.— Lift, hinge-moment, and pitching-moment coefficients of the 35° swept-back tail.
Aspect ratio, 6; $R, 3.0 \times 10^6$.



(b) Hinge-moment coefficient.

Figure 9.—Continued.



(c) Pitching-moment coefficient.

Figure 9.-Concluded.

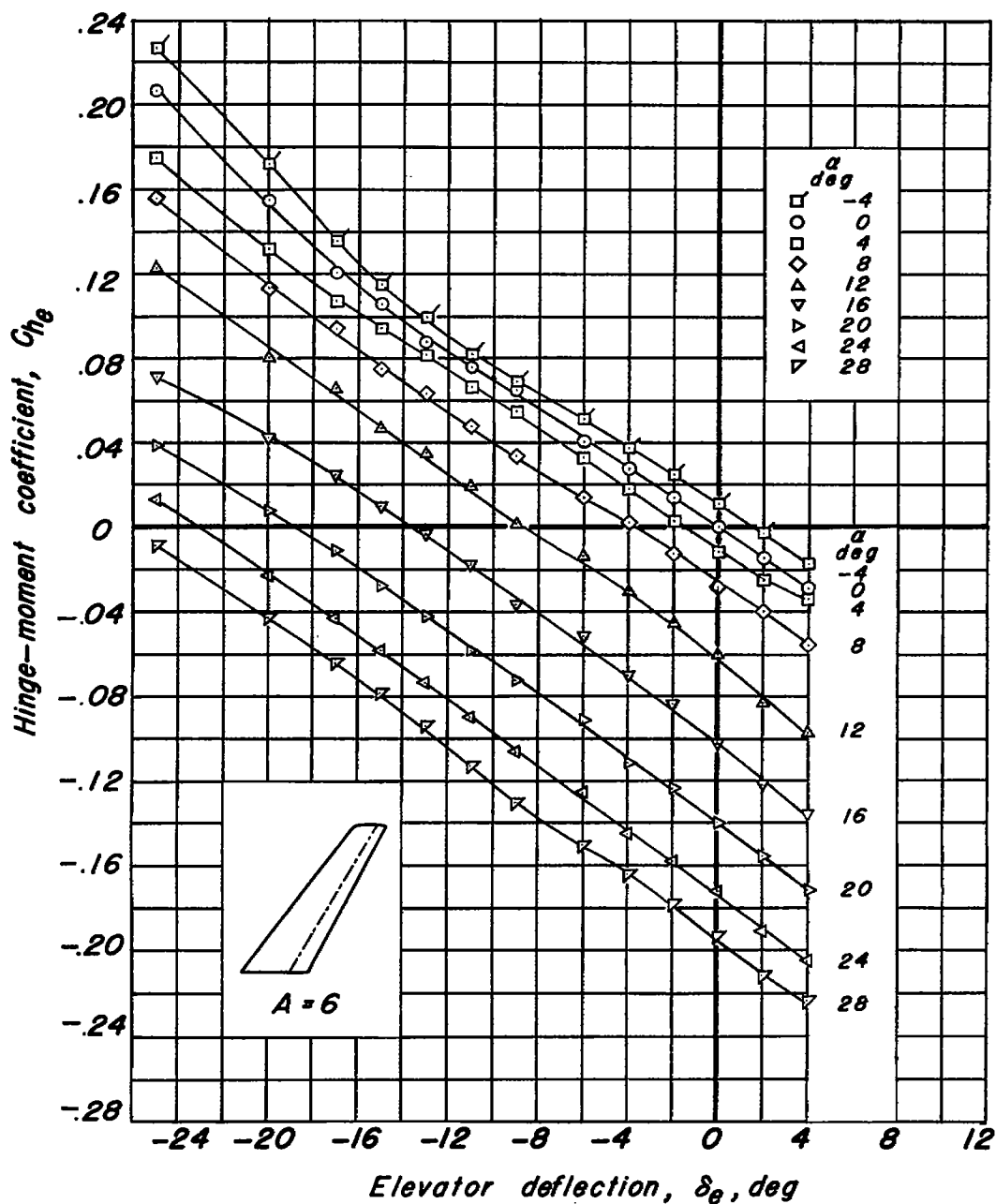
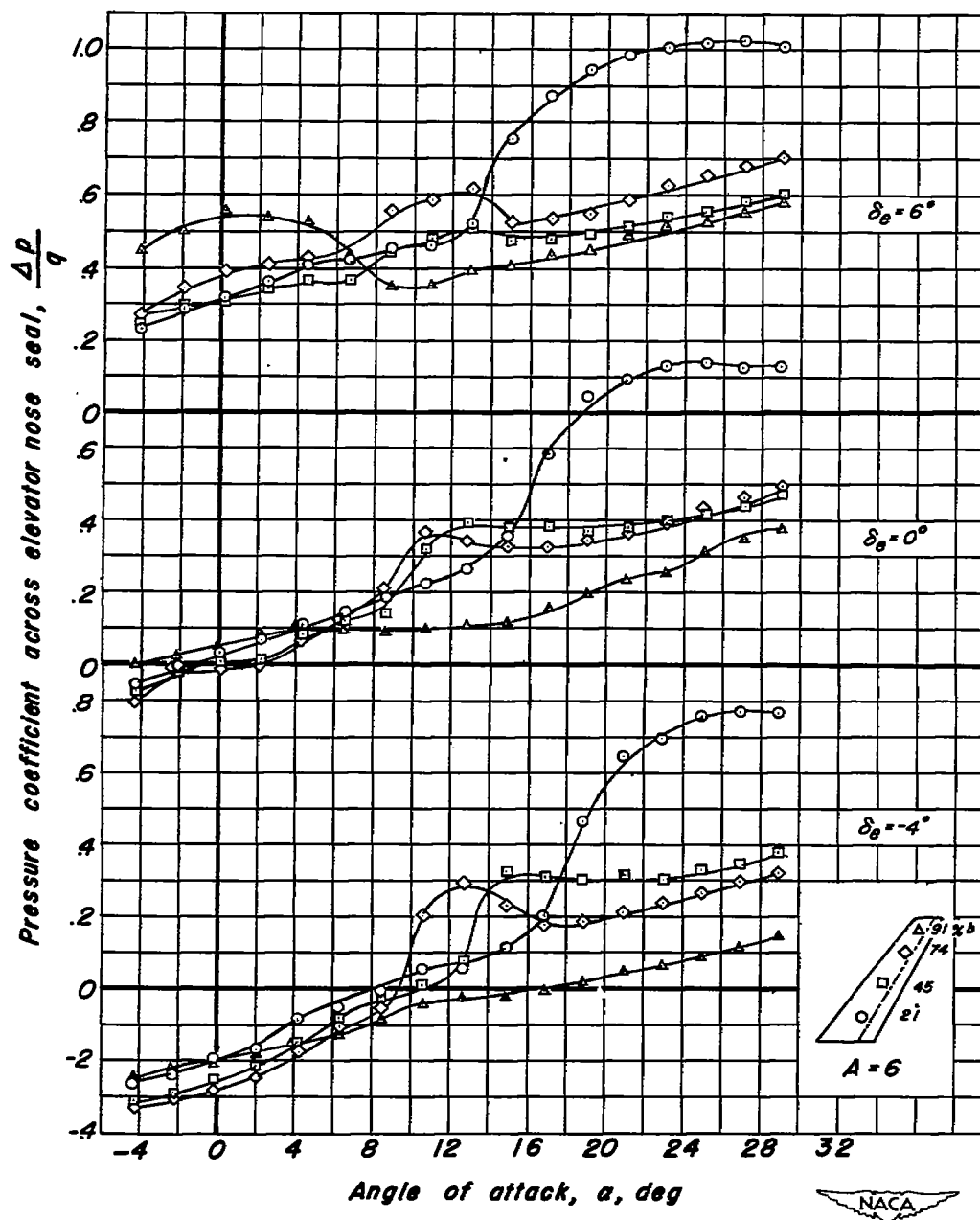
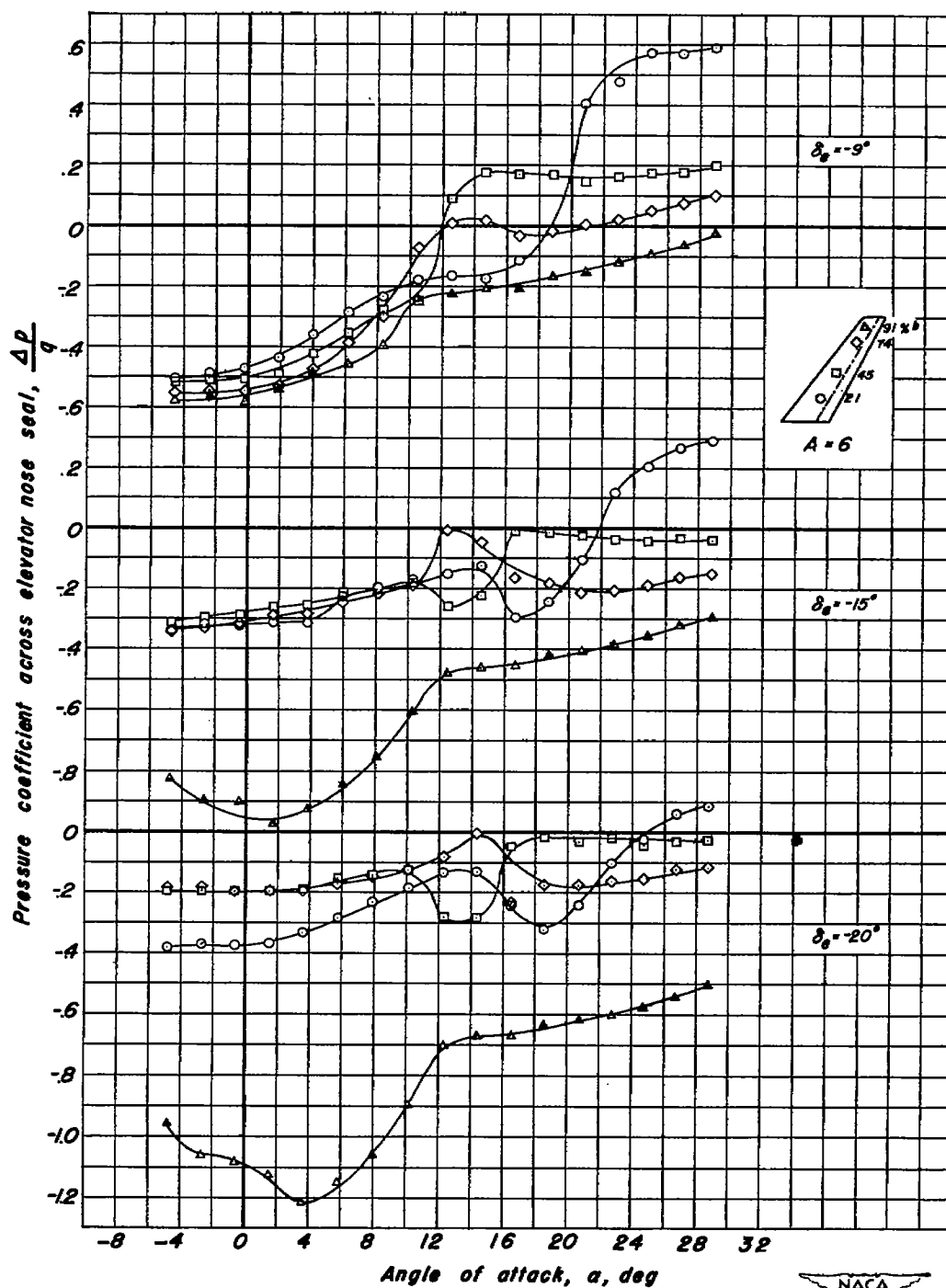


Figure 10.— Variation of hinge-moment coefficient with elevator deflection for various angles of attack of the 35° swept-back tail. Aspect ratio, 6; $R, 3.0 \times 10^6$.



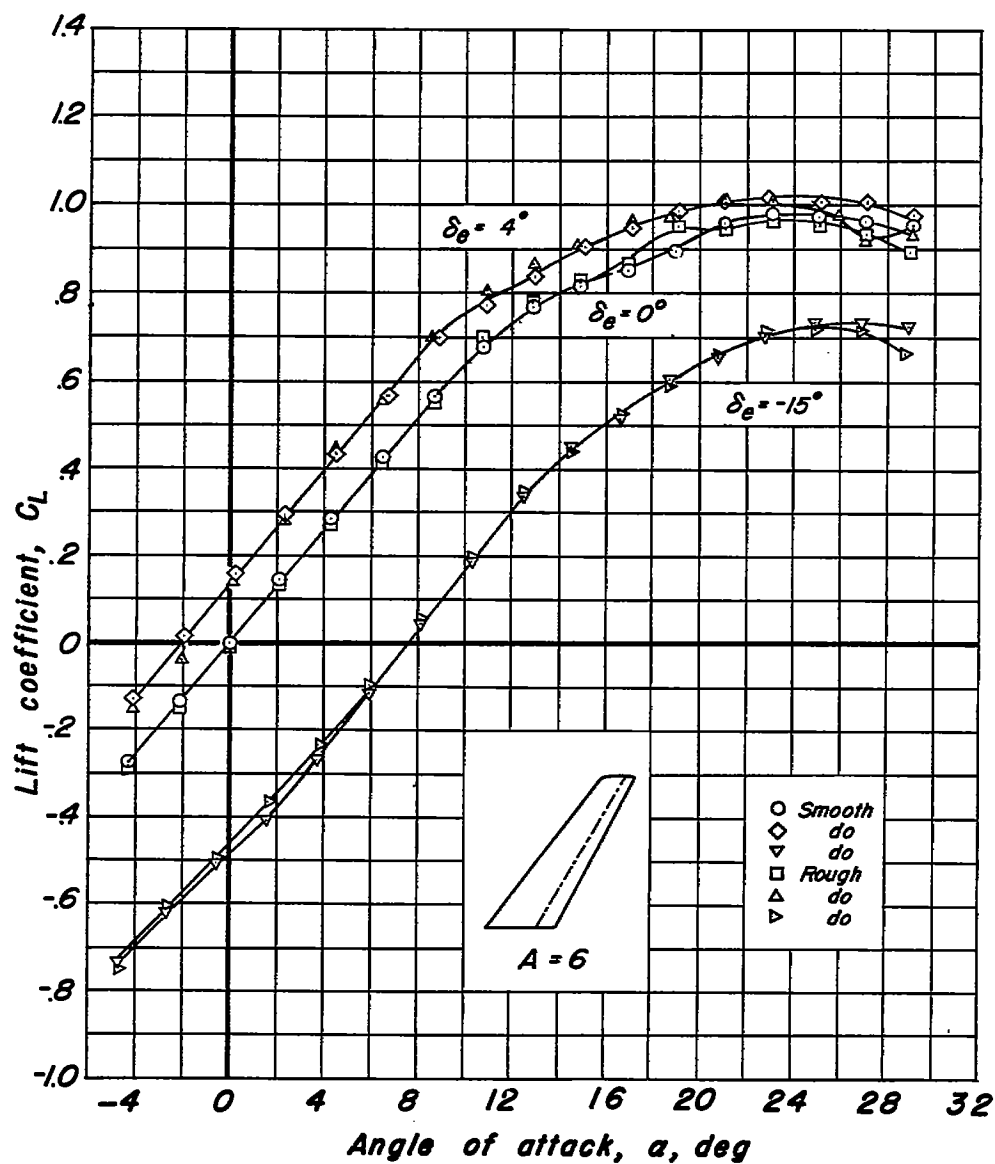
(a) $\delta_e = 6^\circ, 0^\circ, -4^\circ$

Figure 11.— Variation of pressure coefficient across elevator nose seal with angle of attack of the 35° swept-back tail. Aspect ratio, 6; $R, 3.0 \times 10^6$.



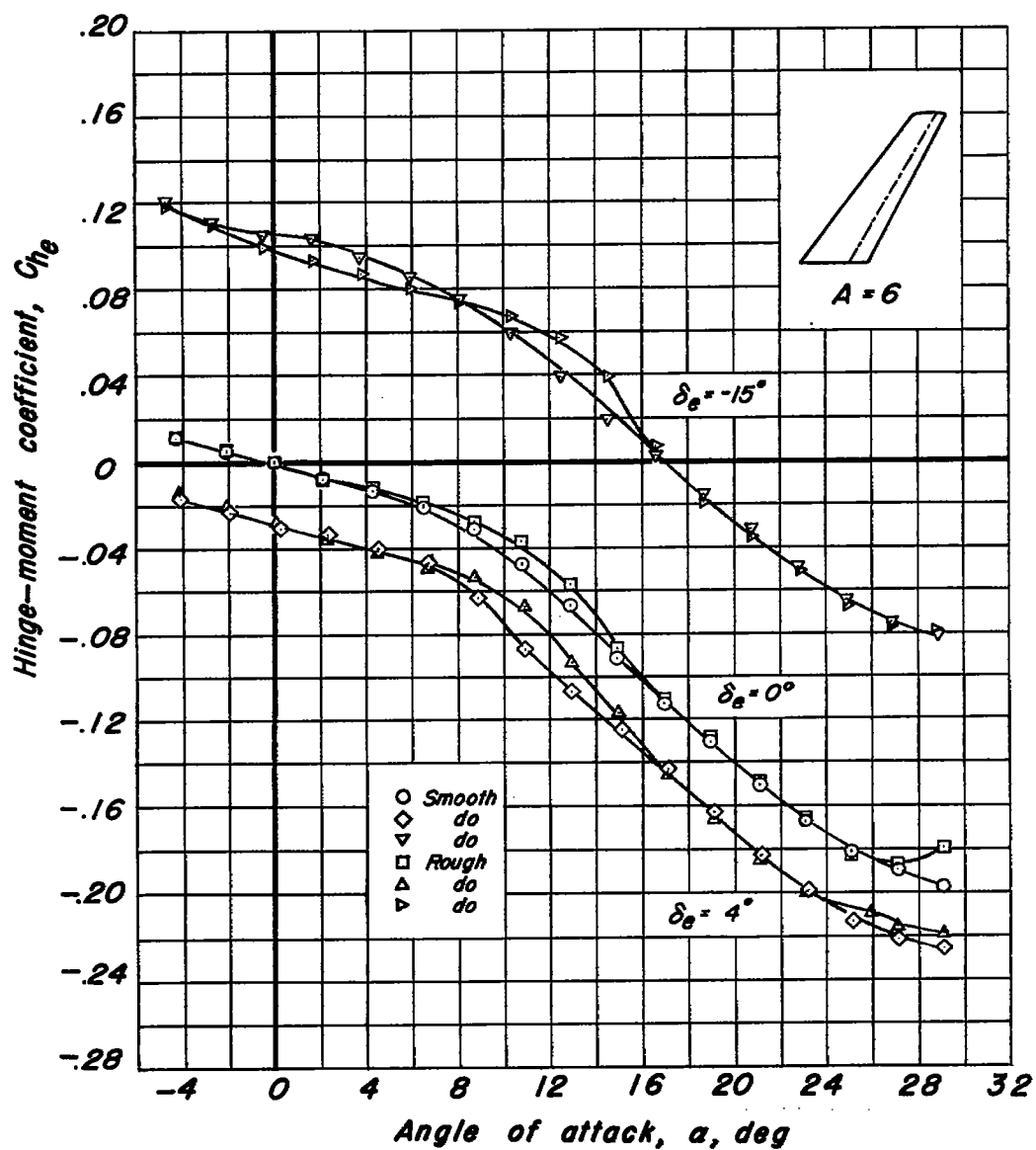
(b) $\delta_0 = -9^\circ, -15^\circ, -20^\circ$.

Figure 11.—Concluded.



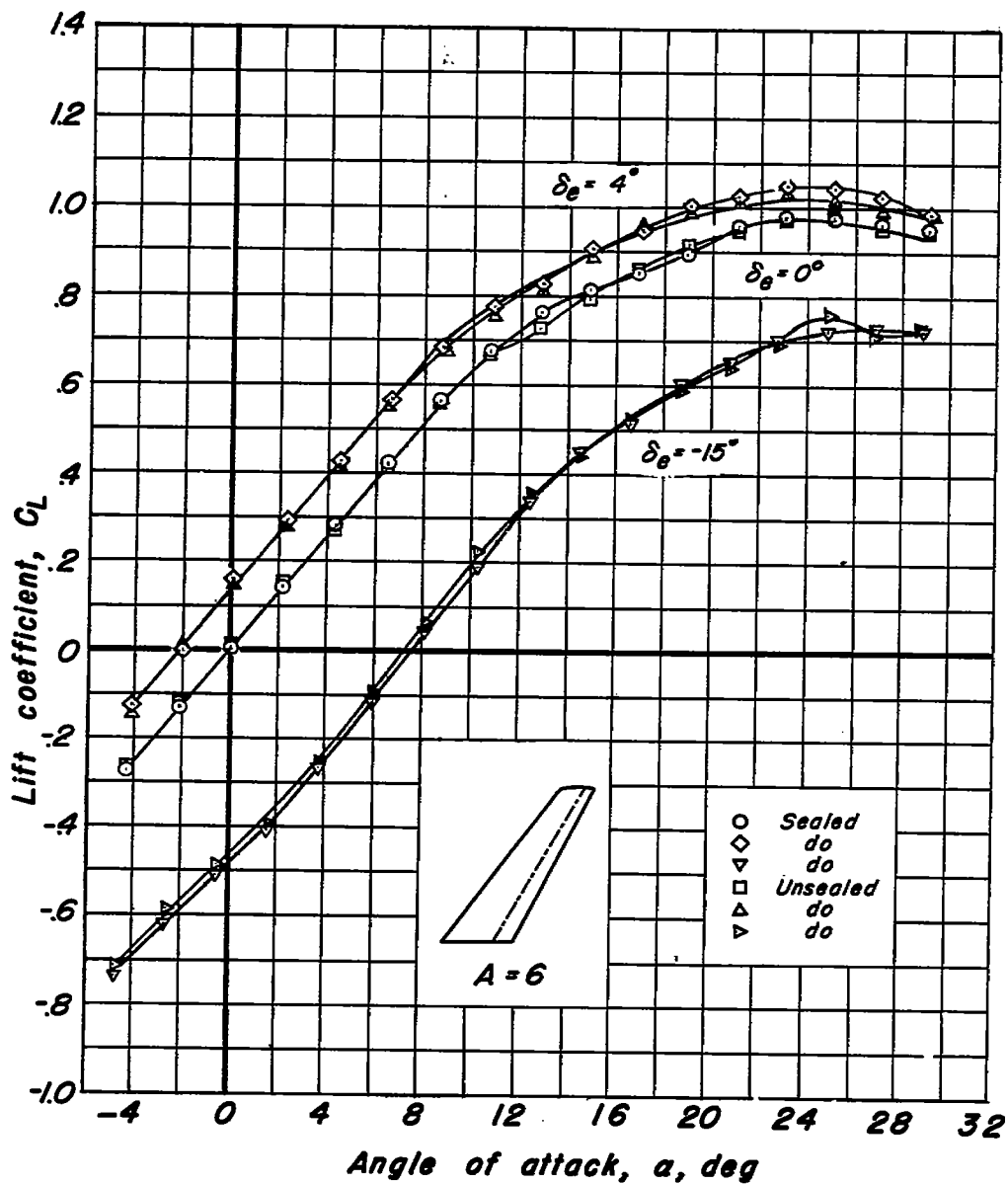
(a) Lift coefficient.

Figure 12.- Comparison of the lift and hinge-moment coefficients with and without leading-edge roughness on the 35° swept-back tail. Aspect ratio, 6; $R, 3.0 \times 10^6$.



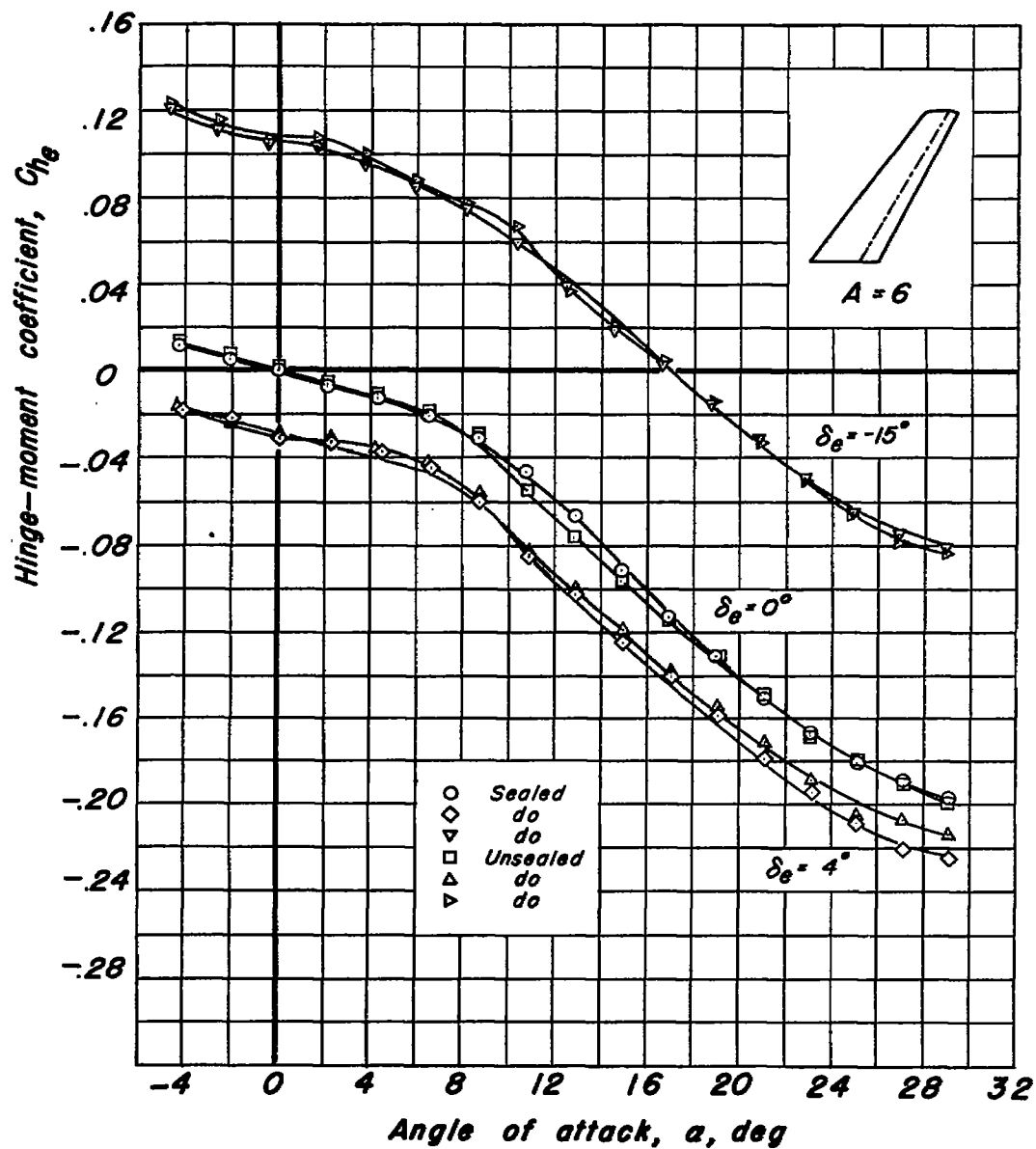
(b) Hinge-moment coefficient.

Figure 12.- Concluded.



(a) Lift coefficient.

Figure 13.- Comparison of the lift and hinge-moment coefficients with and without elevator seal on the 35° swept-back tail. Aspect ratio, 6; $R, 3.0 \times 10^6$.



(b) Hinge-moment coefficient.

Figure 13.—Concluded.

NASA Technical Library



3 1176 01434 4627